JOURNAL OF NEUROTRAUMA 28:535–545 (April 2011)

DOI: 10.1089/neu.2010.1619

Transplantation of Marrow Stromal Cells Restores Cerebral Blood Flow and Reduces Cerebral Atrophy in Rats with Traumatic Brain Injury: *In vivo* MRI Study

Lian Li,[1] Quan Jiang,[1] Chang Sheng Qu,[2] Guang Liang Ding,[1] Qing Jiang Li,[1] Shi Yang Wang,[4] Ji Hyun Lee,[4] Mei Lu,[3] Asim Mahmood,[2] and Michael Chopp[1,4]

Abstract

Cell therapy promotes brain remodeling and improves functional recovery after various central nervous system disorders, including traumatic brain injury (TBI). We tested the hypothesis that treatment of TBI with intravenous administration of human marrow stromal cells (hMSCs) provides therapeutic benefit in modifying hemodynamic and structural abnormalities, which are detectable by *in vivo* MRI. hMSCs were labeled with superparamagnetic iron oxide (SPIO) nanoparticles. Male Wistar rats (300–350 g, $n=18$) subjected to controlled cortical impact TBI were intravenously injected with 1 mL of saline ($n=9$) or hMSCs in suspension ($n=9$, approximately 3×10^6 SPIO-labeled hMSCs) 5 days post-TBI. *In vivo* MRI measurements consisting of cerebral blood flow (CBF), T2-weighted imaging, and 3D gradient echo imaging were performed for all animals 2 days post-TBI and weekly for 6 weeks. Functional outcome was evaluated with modified neurological severity score and Morris water maze test. Cell engraftment was detected *in vivo* by 3D MRI and confirmed by double staining. Ventricle and lesion volumetric alterations were measured using T2 maps, and hemodynamic abnormality was tracked by MRI CBF measurements. Our data demonstrate that treatment with hMSCs following TBI diminishes hemodynamic abnormalities by early restoration and preservation of CBF in the brain regions adjacent to and remote from the impact site, and reduces generalized cerebral atrophy, all of which may contribute to the observed improvement of functional outcome.

Key words: cerebral atrophy; cerebral blood flow; marrow stromal cells; MRI; ventricular expansion

Introduction

As a prevalent cause of neurological morbidity and mortality, traumatic brain injury (TBI) produces primary focal insult and triggers a cascade of complex cellular, molecular, and metabolic events (Stoica and Faden, 2010; Xu et al., 2010; Ziebell and Morgranti-Kossmann, 2010) in the central nervous system (CNS) that lead to diffuse brain damage. Extensive axonal degeneration (Bigler, 1987; Ding et al., 2008; Mamere et al., 2009) and generalized cerebral atrophy (MacKenzie et al., 2002; Sidaros et al., 2009; Trivedi et al., 2007) associated with poor functional outcomes are the common sequelae. TBI-induced hypoperfusion, which could occur beyond the site of primary injury (Bonne et al., 2003; Hofman et al., 2001; Pasco et al., 2007), aggravates this trauma-triggered brain damage. To date, however, the management of patients with TBI has generally concentrated on the prevention or amelioration of such devastating secondary pathological processes since there is no effective clinical treatment (Parr et al., 2007).

Cell transplantation offers an encouraging therapeutic strategy for reversing neurological deficits after CNS injury. Grafted cells play an important role in the repair of injured tissue and also support healing processes after various CNS disorders, such as stroke, intracerebral hemorrhage, spinal cord injury, Parkinson's disease, multiple sclerosis, brain tumor, and TBI (Chopp and Li, 2006; Opydo-Chanek, 2007). Among the types of cells that are employed for treatment purpose, marrow stromal cells (MSCs) are promising due to their potential advantages over others, which include autologous donor, rapid expansion *ex vivo*, and immune privilege (Chopp and Li, 2006; Parr et al., 2007).

Previous laboratory studies on the treatment of TBI with MSCs either from animals or humans showed therapeutic efficacy, as evidenced by significantly improved functional recovery (Lu et al., 2001; Mahmood et al., 2001, 2003).

[1]Department of Neurology, [2]Department of Neurosurgery, [3]Department of Biostatistics and Research Epidemiology, Henry Ford Hospital, Detroit, Michigan.
[4]Department of Physics, Oakland University, Rochester, Michigan.

Although mechanisms responsible for the observed therapeutic potential of MSCs remain to be explored, it is suggested that the beneficial effects are owed to the ability of MSCs to secrete an array of cytokines and trophic factors that activate endogenous restorative and regenerative processes, e.g., angiogenesis, synaptogenesis, gliogenesis, and neurogenesis (Chopp and Li, 2006; Mahmood et al., 2004a, 2004b). Treatment of TBI with transplantation of MSCs may also moderate post-TBI hypoperfusion that results from impaired vasculature or disturbed hemodynamics (Hofman et al., 2001) and may reduce cerebral atrophy that occurs concomitantly with progressive neuronal loss (Immonen et al., 2009a; Smith et al., 1997) and diffuse axonal injury (Bigler, 1987; Ding et al., 2008; Mamere et al., 2009; Sidaros et al., 2009). To our knowledge, however, little is known about the dynamic effect of grafted MSCs on post-TBI hemodynamic and atrophic progression. Magnetic resonance imaging (MRI) is a powerful means for visualizing lesion and for longitudinally and non-invasively monitoring structural and physiological alterations in the living brain (Cunningham et al., 2005; Immonen et al., 2009b, 2010; Kochanek et al., 2002). The present study was designed to test the hypothesis that engraftment of human marrow stromal cells (hMSCs) into the brain subjected to TBI provides therapeutic benefit in modifying cerebral hemodynamic and structural abnormalities, which are detectable by *in vivo* MRI.

Methods

All experiments and procedures involving the use of animals were approved and conducted in accordance with the institutional guidelines for care and use of laboratory animals.

hMSCs and cell labeling

The hMSCs were provided by Theradigm (Baltimore, MD). The cells were labeled *in vitro* with superparamagnetic iron oxide (SPIO) nanoparticles, according to a previously reported method (Li et al., 2010). Briefly, ferumoxide suspension (Feridex IV, Berlex Laboratories, Wayne, NJ) and protamine sulfate (American Pharmaceuticals, Schaumburg, IL) were used to generate ferumoxide-protamine sulfate (Fe-Pro) complexes. Serum-free medium (Biosource, Camarillo, CA), ferumoxide suspension, and protamine sulfate (1 mg/mL in distilled water) at a ratio of 1 mL:100 μg:5 μg were mixed in a flask for 5 to 10 min with intermittent shaking by hand. The cells were incubated in this solution containing Fe-Pro complexes for 2 h. Then, complete medium was added to obtain a final concentration of 50 μg/mL for ferumoxide and 2.5 μg/mL for protamine sulfate, respectively. The cell suspension was incubated overnight at 37°C in a 5% CO_2 humidified atmosphere to allow the nanoparticles to infuse into the cells and thereby label them. Prior to injection into rats, the labeled cells were suspended in phosphate-buffered saline (PBS).

SPIO-labeled hMSCs were checked for viability via Trypan blue exclusion. The tests demonstrated that more than 95% of the cells remained viable after labeling with SPIO.

Animal model and cell transplantation procedures

All surgical procedures were conducted under aseptic conditions. Male Wistar rats (300–350 g, $n=18$) were intraperitoneally anesthetized with chloral hydrate (350 mg/kg body weight), and rectal temperature was maintained at 37°C with a feedback-regulated water heating pad. The head of each animal was mounted in a stereotactic frame and two 10-mm-diameter craniotomies were performed adjacent to the central suture, midway between the lambda and the bregma, leaving the dura mater over the cortex intact. The left craniotomy confined the location of experimental impact while the right one allowed the lateral movement of cortical tissue. Using a controlled cortical impact (CCI) device, brain injury was induced by delivering a single impact at a rate of 4 m/sec and 2.5 mm of compression to the left cortex with a pneumatic piston containing a 6-mm-diameter tip. All animals that underwent TBI survived. For analgesia, Buprenex (0.05 mg/kg, s.q.) was administered to each animal after brain injury.

Cell transplantation was conducted 5 days after TBI. The 5-day time point for cell transplantation after TBI has been shown previously to provide significant functional improvement (Li et al., 2010; Lu et al., 2007; Xiong et al., 2009), and this timing is after the intense inflammatory response of the trauma-injured brain (Assaf et al., 1997; Soares et al., 1992). Rats subjected to TBI were randomized to one of two treatment groups—cell and saline treated. Anesthesia was reinstituted before the transplantation and a bolus of the cell suspension (approximately 3×10^6 SPIO-labeled hMSCs in 1 mL PBS) was slowly infused over a 5-min period into the tail vein of each rat in the cell-treated group ($n=9$) using a Hamilton syringe. The needle was left in place for 1 min before withdrawal to minimize cell leakage and the injection site was compressed for a short time to reduce bleeding. Replacing the cell suspension with the same amount of saline, each animal in the saline-treated group ($n=9$) underwent the identical procedure as those in the cell-treated group. No immunosuppressants were used in this study.

In vivo *MR imaging*

MR imaging was performed using a 7T, 20 cm-bore superconducting magnet (Magnex Scientific, Abingdon, United Kingdom) interfaced to a Bruker console (Bruker, Boston, MA). The animal was securely fixed on a non-magnetic holder equipped with a nose cone for administration of anesthetic gases and stereotaxic ear bars to minimize movement of the head. A tri-pilot scan of imaging sequence was used for reproducible positioning of the animal in the magnet at each MRI session. During the imaging procedure, anesthesia was maintained with 1.0% halothane in 69% N_2O and 30% O_2, and rectal temperature was kept at 37°C ± 1.0°C using a feedback-controlled water bath underneath the animal. T2-weighted imaging (T2WI), cerebral blood flow (CBF), and high-resolution three-dimensional (3D) gradient echo imaging were measured for all animals 2 days post-TBI, and then the identical measurements were repeated once a week for 6 weeks. All rats were euthanized after final *in vivo* MRI scans.

T2WI was acquired using standard two-dimensional multi-slice (13 slices, 1 mm thick), multi-echo (6 echoes) sequence. Six sets of images (13 slices per set) were obtained using echo times (TE) of 15, 30, 45, 60, 75, and 90 msec and a repetition time (TR) of 8 sec. Images were obtained using a 32×32 mm^2 field of view (FOV) and a 128×64 image matrix.

The continuous arterial spin-labeling technique was used to quantify CBF in cerebral tissue. Adiabatic inversion of arterial water protons was accomplished via an axial gradient of 0.3 kHz/mm and a 1-sec continuous radio frequency power

wave of approximately 0.3 kHz at a frequency offset of 6 kHz. This was followed by a spin echo imaging sequence with TR/TE = 1,000/20 msec. The labeled slice was 2 cm distal from the imaging slice which was 1 mm thick. In order to eliminate gradient asymmetry in the axial direction, an image average was applied by switching around the gradient polarities. FOV was $32 \times 32\ mm^2$ and the image matrix was 64×64.

3D gradient echo images were acquired with TR of 40 msec, TE of 10 msec, flip angle of 15°, and a $32 \times 32 \times 24\ mm^3$ FOV. The $256 \times 192 \times 64$ image matrix was interpolated to $256 \times 256 \times 64$ for analysis.

MRI data processing

Ventricle and TBI-induced focal lesions present as marked hyperintensities on T2 maps (Figs. 1 and 2). Over time, following TBI, these two distinct regions with elevated T2 values could become contiguous with (Fig. 2B) or without (Figs. 1A and 2A,E) blurry edges, particularly at the later stage of TBI. Under such circumstances, it was impossible to distinguish between them using only the T2 map (Fig. 1A). However, the structural information revealed by 3D image, such as corpus callosum (Fig. 1B, red arrowheads), provided a borderline that divided the hyperintense area detected on T2 map (Fig. 1C, red track) into focal lesion and expanded ventricle (Fig. 1D). 3D images were first co-registered with T2 maps. Region of interest (ROI) encompassing both lesion and ipsilateral ventricle on T2 map was then copied onto the corresponding 3D image where the borderline (Fig. 1D, blue line) was manually added within the ROI. The demarcation was performed on each T2 slice with connected cortical lesion and expanded ventricle.

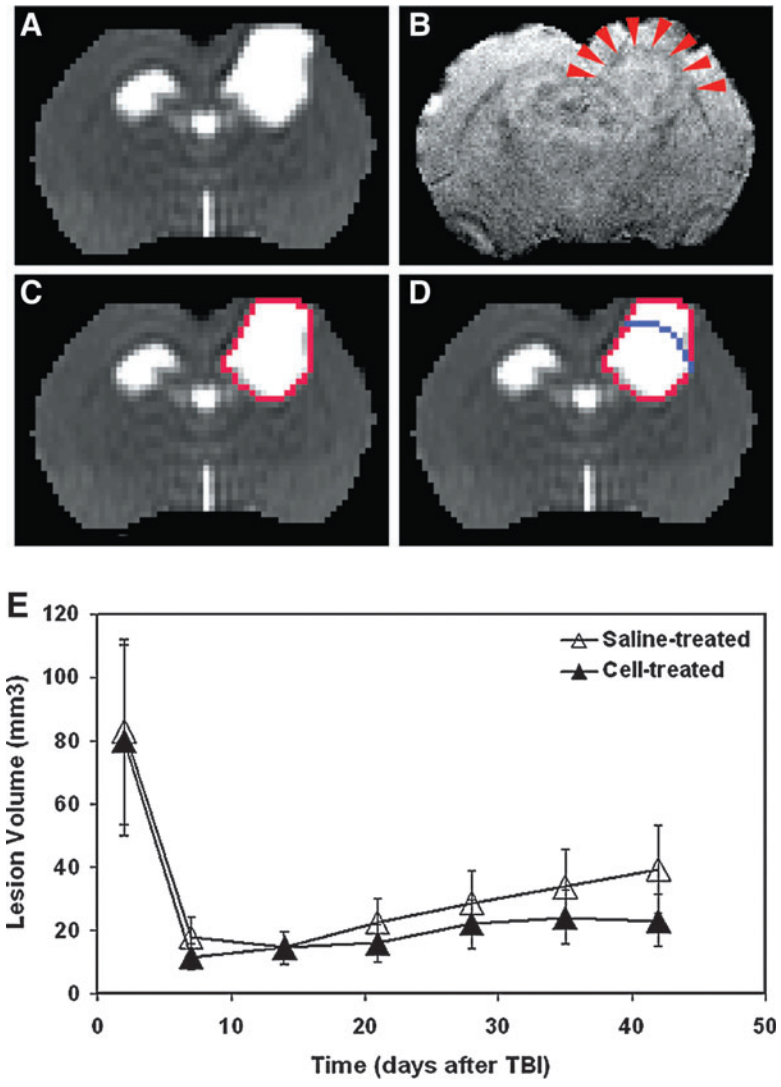

FIG. 1. A representative saline-treated animal with a controlled cortical impact lesion and expanded lateral ventricle after TBI detected by T2 map (**A**) and corresponding 3D image (**B**). When using mean + 2SD threshold, a hyperintense area encompassing both lesion and ipsilateral ventricle were identified on the T2 map (**C**, red track). It was impossible to distinguish between them using only the T2 map. However, the anatomical information revealed by the 3D image (**B**), such as corpus callosum (**B**, red arrowheads), provided a borderline (**D**, blue line) that divided the hyperintense area identified on T2 map into two regions, upper cortical lesion and lower expanded ventricle (**D**). No significant group difference in T2 lesion volume was found over a 6-week observation period (**E**).

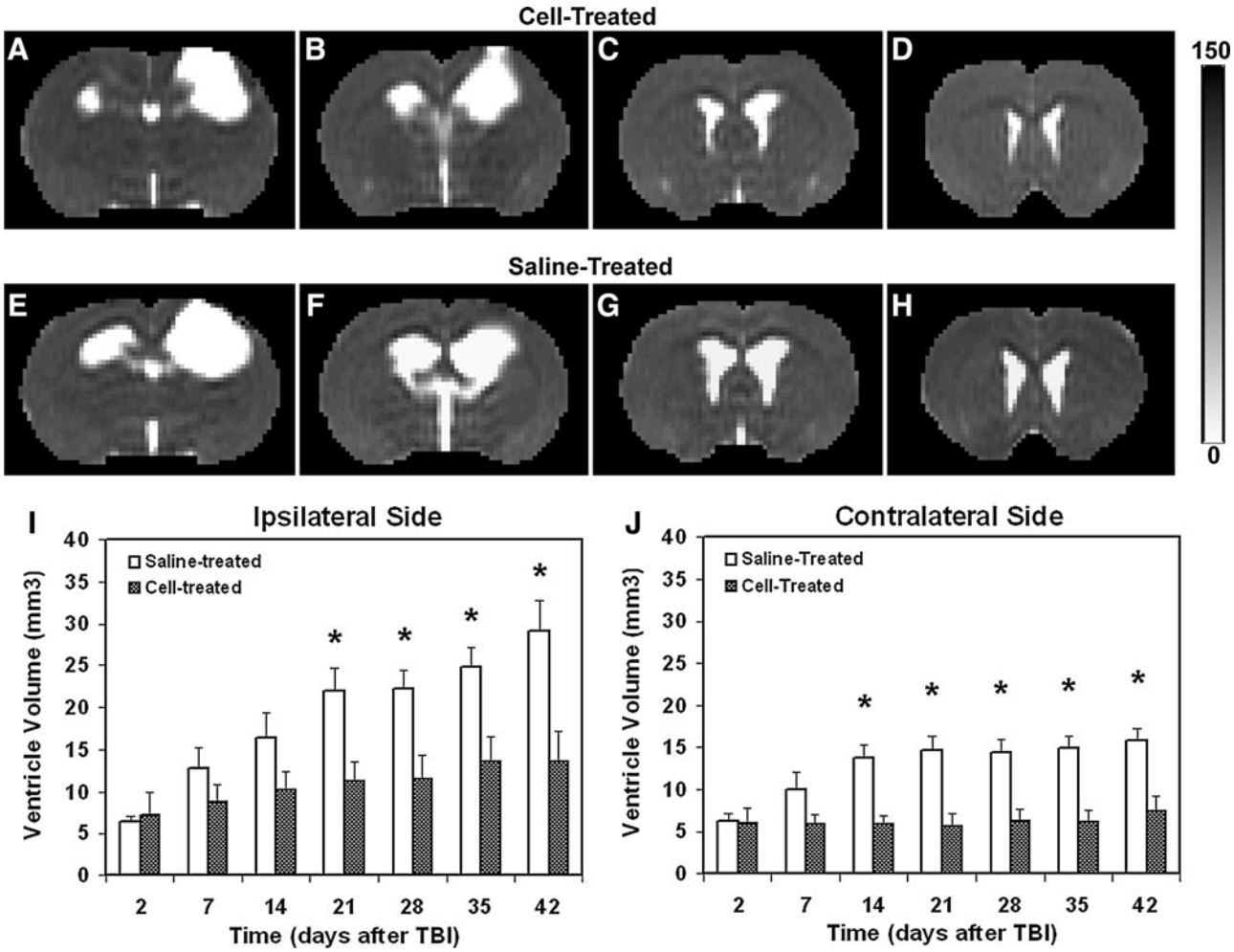

FIG. 2. Comparison of lateral ventricle (6 weeks post-TBI) presented by four consecutive T2 slices (**A**–**D**, cell-treated animal; **E**–**H**, saline-treated animal) and quantitative results (**I**,**J**). Saline-treated animals had a significantly larger ventricle in the ipsilateral (**I**, 3–6 weeks, $p < 0.02$) and contralateral sides (**J**, 2–6 weeks, $p < 0.003$) of the brain after TBI than cell-treated animals. Ipsilateral ventricle was more affected by TBI than the contralateral ventricle for both treatment groups (compare **I** with **J**). Treatment with cell transplantation significantly reduced both the magnitude ($p < 0.03$) and rate ($p < 0.04$) of ventricular expansion after TBI.

Generated T2 maps (13 equally spaced coronal slices) covered the entire rat brain. The lesion area on each slice of T2 map was specified by those pixels with a T2 value higher than the mean plus twice the standard deviation (mean + 2SD) provided by the normal tissue on the contralateral (non-injured) side (Li et al., 2005). Lesion volume was then calculated on the basis of lesion areas on individual slices and slice thickness.

As shown in Figure 2, the volume of the lateral ventricle was measured on T2 maps at a fixed structural location presented by four contiguous coronal slices for all animals (approximately at the level of bregma −2.8 to bregma 1.2). The same criterion described above was used to identify the ventricular area on each slice. Similarly, the volume was obtained by adding all the areas measured on individual slices and multiplying the total by the slice thickness. Data are presented as ventricle volumes in the ipsilateral and contralateral sides of the brain.

To quantify TBI-induced hypoperfusion, a threshold for CBF (30mL/100 g/min) derived from experimental ischemia (Shen et al., 2004) was used to detect the location and extent of tissue regions with perfusion abnormality. Areas with CBF lower than this threshold were identified on the CBF map (ventricles were excluded) and presented as percentage of the examined slice.

Measurements were performed for each animal in both cell- and saline-treated groups and the data were averaged at the same time points for each group.

Modified neurological severity score

The modified neurological severity score (mNSS) (Xiong et al., 2009) grades the composite neurological function of an animal on motor, sensory, reflex, and balance tests. The maximum points for each category of tests are 6, 2, 4, and 6, respectively. One point is awarded for the inability of an animal to perform the tasks correctly or for the lack of a tested reflex (normal score, 0; maximal deficit score, 18). Therefore, the higher score indicates the more severe neurological dysfunction (13–18, severe injury; 7–12, moderate injury; 1–6,

mild injury). mNSS was assessed for each animal pre-TBI and post-TBI on days 1, 4, and weekly thereafter by an examiner blinded to the treatment groups and the corresponding MRI results.

Modified Morris water maze test

To evaluate the long-term functional outcome of spatial learning acquisition and memory retention, the modified Morris water maze (Mahmood et al., 2007) was used. The testing system consisted of a circular tank (140 cm in diameter and 45 cm high) filled with 30°C water and a hidden platform (15 cm in diameter and 35 cm high) set inside the tank 1.5 cm below the surface of the water. The pool was located in a large test room decorated with visual clues (for example, pictures, lamps, and so forth) that remained constant during the study and enabled the rats to orientate themselves spatially. For descriptive data collection, an automated tracking system (HVS Image, San Diego, CA) was employed and the pool was subdivided into four equal quadrants formed by imaging lines.

The rats were tested on 5 consecutive days (1 trial per day) at the later stage of TBI (from day 31 to 35 after TBI). Each trial was initiated by placing the animal randomly at one of four start locations (north, south, east, and west) and allowing 90 sec to find the hidden platform. The platform was put in a randomly changing position within the northeast (NE) quadrant throughout the test period (e.g., sometimes equidistant from the center and edge of the pool, against the wall, near the center of the pool, and at the edges of the NE quadrant). After locating the platform, the animal was allowed to remain on the platform for 15 sec before being returned to its cage. If the animal failed to find the platform within 90 sec, the experiment was terminated and a maximum score of 90 sec was assigned. The percentage of time traveled within the NE (correct) quadrant was calculated relative to the total amount of time swimming before reaching the platform.

Tissue preparation and histology

Immediately after the final *in vivo* MRI measurements at 6 weeks after TBI, rats were deeply anesthetized with ketamine (44 mg/kg, i.p.) and xylazine (13 mg/kg, i.p.) and transcardially perfused with heparinized saline, followed by 4% paraformaldehyde. The brains were removed shortly after death, placed in 4% paraformaldehyde in PBS at 4°C for 2 days, and then cut into seven standard coronal blocks 2 mm thick on a rodent brain matrix. Coronal sections 6 μm thick were sliced from each block embedded in paraffin and stained for histological evaluation.

To detect labeled hMSCs in the host brain, tissue sections were stained for iron using Prussian blue reaction (Li et al., 2010). The coronal tissue sections were deparaffinized, rinsed in de-ionized water, and incubated for 30 min with 2% potassium ferrocyanide (Perls' reagent) in 6% HCl, then washed well with distilled water, and counterstained with nuclear fast red.

To confirm that the PB-positive cells were the grafted human cells (hMSCs), we performed double staining with antibodies specifically against human mitochondria (E5204, Spring Bioscience, CA) and Prussian blue. The tissue sections were then photomicrographed to show the co-localization of double-positive cells.

Statistical analysis

A mixed model, analysis of variance and covariance, was employed to compare the group difference in MRI measurements (hypoperfusion area, lesion, and ventricle volumes) and functional assessments (mNSS and water maze test). Analysis began with testing the treatment group and time interaction, followed by testing the group difference at each time point and the time effect for each treatment group if the interaction or the overall group/time effect was detected at the 0.05 level. A subgroup analysis would be considered if the interaction or main effect of group/time was not at the 0.05 level. Pearson correlations were calculated at each time point among MRI measurements and between MRI measurements and functional assessments adjusted for treatment groups. A p value of ≤ 0.05 was used to denote statistical significance.

Results

Volumetric change of TBI lesion on T2 map

TBI caused transient edema over a wide range extending from the primary impact site. The permanent focal lesion was localized to the cortical region, and in some cases in the underlying hippocampal region, and was identified as a hyperintensity on the T2 map (Fig. 1A). The temporal profiles of lesion volume depicted on T2 map were similar for the two treatment groups (Fig. 1E), with a large edematous tissue volume appearing acutely, then rapidly decreasing to a focal lesion within 1 week and gradually extending from 1 to 6 weeks. No significant group differences in T2 lesion volume were found over a 6-week observation period.

Ventricular expansion following TBI

Structural alteration characterized by ventricular enlargement after TBI was detected in both cell- and saline-treated animals (Fig. 2). As visualized by T2 maps, this structural abnormality was particularly marked in the hemisphere ipsilateral to the primary injury. However, ventricular expansion in both sides of the brain was less evident in the cell-treated animal compared with the saline-treated animal (compare Fig. 2A–D with Fig. 2E–H in the ventricle area). Statistical analysis showed that a significant time effect of ventricular enlargement in the ipsilateral (Fig. 2I) and contralateral sides (Fig. 2J) of the brain was found in the saline-treated group ($p < 0.001$) but not in the cell-treated group ($p > 0.17$). At 2 days after TBI, no statistical difference in ventricle volume (ipsilateral and contralateral sides) between the groups was detected (Fig. 2I–J; $p > 0.85$). There was a progressive increase in ventricle volume starting 1 week after TBI for both treatment groups, and the ventricular dilation in the saline-treated group continued steadily for several weeks thereafter at a longitudinal rate greater than that observed in the cell-treated group (ipsilateral side, 3.30 ± 0.65 vs. $1.27 \pm 0.62 mm^3$/week; contralateral side, 1.33 ± 0.28 vs. $0.54 \pm 0.24 mm^3$/week; $p < 0.04$). As a result, saline-treated animals had a significantly larger ventricle in the ipsilateral (Fig. 2I; 3–6 weeks, $p < 0.02$) and contralateral sides (Fig. 2J, 2–6 weeks, $p < 0.003$) of the brain after TBI than cell-treated animals. As shown in Figure 2I, J, ipsilateral ventricle was more affected by TBI than the contralateral ventricle for both treatment groups. Treatment with cell transplantation significantly reduced the magnitude ($p < 0.03$) and rate ($p < 0.04$)

of ventricular expansion after TBI (group and time effect, $p < 0.05$). This overall cell effect ($p < 0.05$) was detected in both the ipsilateral (Fig. 2I) and contralateral ventricles (Fig. 2J).

Hypoperfusion after TBI

In Figure 3, a comparison of CBF maps between the two treatment groups is illustrated by representative animals. In the lesion site, a larger affected area with lower CBF was present in the saline-treated animal than in the cell-treated animal after TBI (compare Fig. 3A–C with Fig. 3D–F). Our consecutive observations over a 6-week period showed that TBI-induced hypoperfusion occurred at the site of direct mechanical injury and also in the remote regions. While the area with lower CBF extended beyond the location of primary impact site (Fig. 3D–F), treatment with cell transplantation restored and preserved CBF in the brain regions adjacent to and remote from the lesion (Fig. 3A–C) at a later stage of TBI. In agreement with this observation, statistical results showed that a significant time effect of hypoperfusion area was detected in the cell-treated group only ($p < 0.001$; in the saline-treated group, $p > 0.30$). Consistently, temporal profiles of areas with lower CBF also distinguished the saline- from the cell-treated groups (Fig. 3G). At acute and subacute times, no statistical difference in the area with lower CBF between two groups was found. The hypoperfused area gradually decreased afterwards in the cell-treated group with significant reduction achieved at 3 weeks as compared with 2 days post-TBI ($p < 0.03$) and persisting thereafter, while the area of hypoperfusion did not change significantly in the saline-treated group during the same period. Consequently, a significantly larger area with abnormal CBF value (lower than 30 mL/100 g/min) was detected in the saline-treated group than in the cell-treated group at the later stage of TBI (Fig. 3G; 3–6 weeks, $p < 0.03$).

Grafted cells and hemorrhage in the injured brain

Prussian blue staining demonstrated that the iron-positive cells primarily localized adjacent to the lesion site and included the cortex, striatum, and corpus callosum (CC) regions, which matched the hypointense areas on 3D image (Fig. 4B–F). Double staining confirmed that these PB-positive cells (Fig. 4G, dark cells, left arrows) identified in the lesion boundary region were the grafted hMSCs (Fig. 4G, red cells, right arrows). The areas with reduced signal intensity sur-

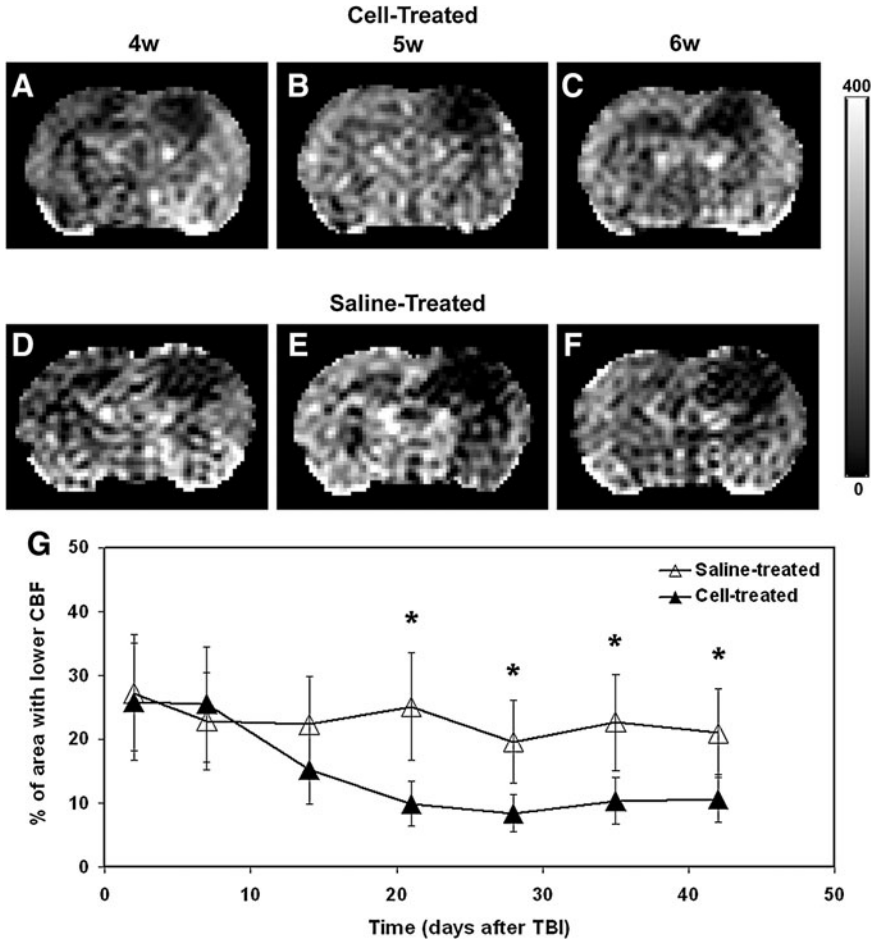

FIG. 3. Illustrative comparison of CBF maps shown in representative animals (**A–C**, cell-treated animal; **D–F**, saline-treated animal) and quantitative results (**G**). While the area with lower CBF extended beyond the location of the primary impact site (**D–F**), treatment with cell transplantation restored and preserved CBF in the brain regions adjacent to and remote from the lesion (**A–C**) at a later stage of TBI. A significantly larger area with lower CBF value (lower than 30 mL/100 g/min) was detected in the saline-treated group than in the cell-treated group at a later stage of TBI (**G**, 3–6 weeks, $p < 0.03$).

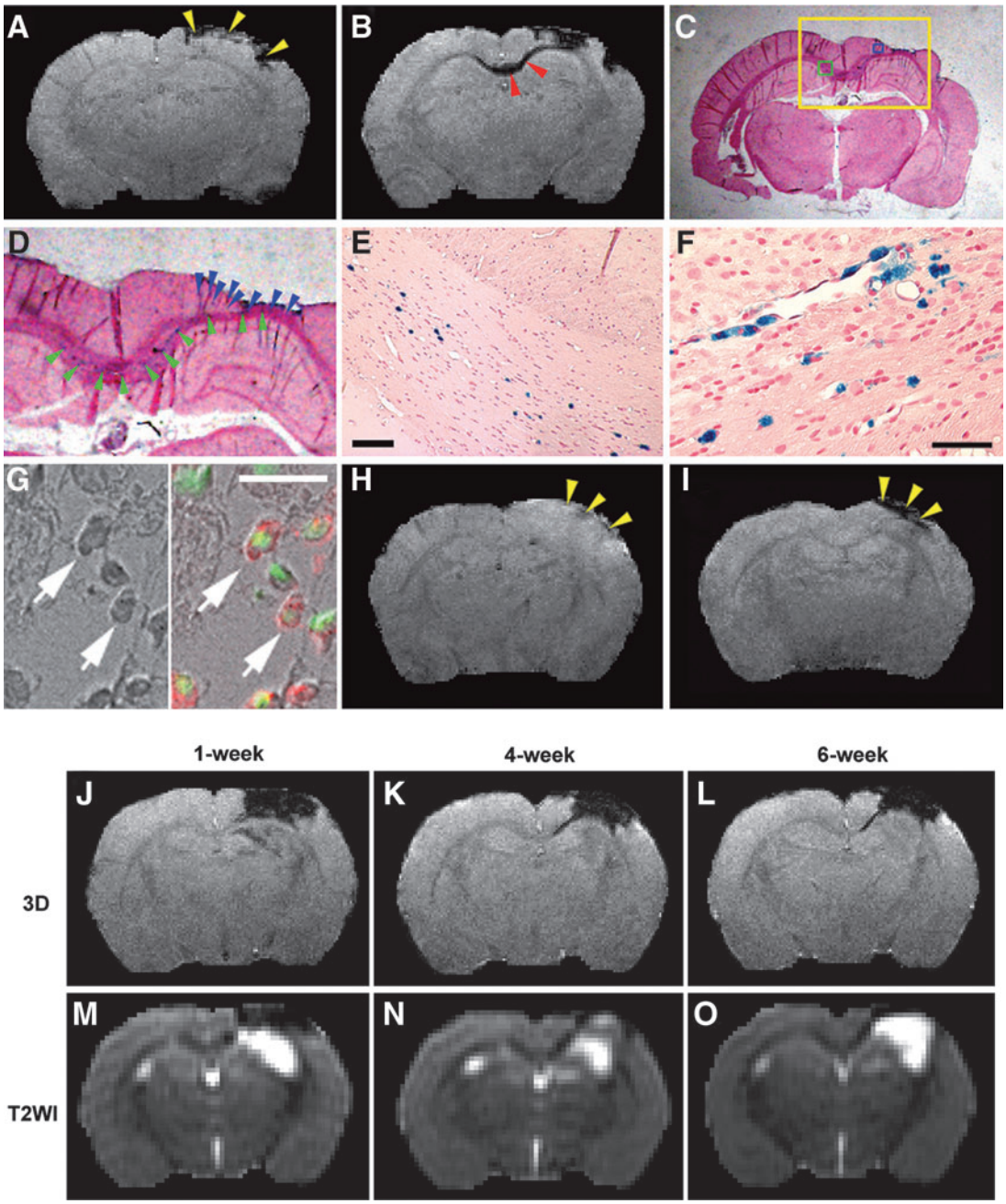

FIG. 4. Grafted cells and intracranial hemorrhage shown in representative animals (**A**–**G**, **J**–**O**, cell-treated animals; **H**,**I**, saline-treated animal). Areas with signal reduction on 3D image at or near the impact site (**A**, yellow arrowheads), which appeared prior to the cell engraftment (2 days post-TBI), were caused by hemorrhage. With time, traumatic lesion was present in the cortical region and finally became cystic as confirmed by histological slice (**C**, PB staining). **D**–**F** give higher magnification of local view (**D**) and micrographs (**E**,**F**) obtained from yellow, green, and blue boxes illustrated in **C**, respectively. After cell administration, hypointensity in the CC region (**B**, red arrowheads, 2 weeks post-TBI) and lesion boundary zone (**B**, larger hypointense area in cortex compared to **A**) appeared on 3D image (**B**), which matched the location of PB-positive cells identified on the corresponding tissue slice (**D**, green and blue arrowheads). Double staining (**G**, left, bright field image; right, merged image) showed that these PB-positive cells (dark in **G**, left arrows) were the grafted hMSCs (red in **G**, right arrows) with single nuclei indicated by DAPI (green in **G**, right arrows). Compared with the cell-treated animal (**A**,**B**), hypointensity on 3D images (intracerebral hemorrhage) for the saline-treated animal (**H**,**I**, 2 days and 2 weeks post-TBI, respectively) was detected in the impact site (**H**,**I**, yellow arrowheads), but no dampening signals developed in the CC region at the later time point (compare **I** with **B** in the CC region). Scale bar = 100 μm for **E**,**F**; 20 μm for **G**. Although both hemorrhage and labeled cells caused hypointensity on 3D image (**J**–**L**), MR signal evolution patterns of them on T2WI (**M**–**O**) were different, which distinguished the site with intracerebral hemorrhage from the region with SPIO-labeled cells. At 1 week post-injury, hypointensity in hemorrhagic cortical region on T2WI indicated deoxyhemoglobin (**M**). After 4 weeks (**N**), deoxyhemoglobin converted to methemoglobin (hyperintensity within the hemorrhagic area) with iron storage products deposited at the periphery (rim of hypointensity). As methemoglobin was metabolized, a cystic lesion formed (**O**, hyperintensity in cortex). However, this distinctive evolution pattern in hemorrhagic area on T2WI was absent in the region with SPIO-labeled cells (such as **M**–**O** in the CC region).

rounding the lesion site on 3D image, indicating the presence of grafted SPIO-labeled hMSCs, appeared within 1 week after cell transplantation and were persistently observed in the same location *in vivo* up to 6 weeks after TBI.

Prior to the cell engraftment, pronounced hypointense signals on 3D image at or near the impact site (Fig. 4A, yellow arrowheads) were also observed soon after TBI in both treatment groups. The areas with marked signal dampening appeared between the injured cortex and the underlying hippocampus or around the tissue region subjected to the primary impact. This type of signal loss resulted from a local hemorrhage induced by impact compression and contusion (Immonen et al., 2009a). Of 18 injured animals, intracerebral hemorrhage with various extent occurred in16 brains (89%, $n = 8$ per group).

Although both hemorrhage and labeled cells caused hypointensity on 3D image (Fig. 4J–L), the biochemical state of hemoglobin detected by T2WI (Morris, 2002) (Fig. 4M–O; TR/TE = 8000/60) distinguished the site with intracerebral hemorrhage from the region with SPIO-labeled cells. At 1 week post-injury, hypointensity in the hemorrhagic cortical region was observed on T2WI (Fig. 4M), indicative of deoxyhemoglobin. After 4 weeks, deoxyhemoglobin further converted to methemoglobin with iron storage products deposited at the periphery (Morris, 2002). This was presented on T2WI (Fig. 4N) as hyperintensity (methemoglobin) within the hemorrhagic area surrounded by a thin irregular rim of marked hypointensity (hemosiderin, ferritin). As methemoglobin was resorbed or metabolized, a collapsed cleft followed by a cystic lesion formed (Fig. 4O, hyperintensity in cortex). However, this distinctive evolution pattern in hemorrhagic area on T2WI was absent in the region with SPIO-labeled cells, such as the CC area, which exhibited persistent signal intensity on both 3D image (Fig. 4K,L) and T2WI (Fig. 4N,O) within the observation period.

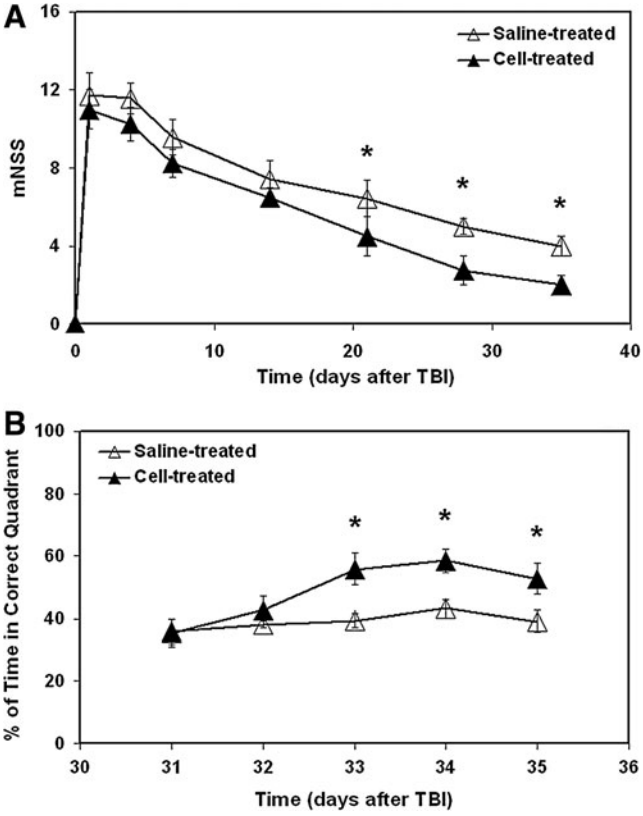

FIG. 5. Functional outcome after TBI. Significantly higher mNSS numbers were awarded to the saline-treated animals than to the cell-treated animals (**A**, 3–5 weeks, $p < 0.03$). The cell-treated animals spent significantly longer time in the correct quadrant than the saline-treated animals (**B**, 33–35 days, $p < 0.05$).

Outcome of neurological function after cell treatment

An improved functional performance, as measured by mNSS and water maze test, was detected in the cell-treated group compared to the saline-treated group (Fig. 5A,B). Significantly higher mNSS numbers were awarded to the saline-treated animals than to the cell-treated animals (Fig. 5A; 3–5 weeks, $p < 0.03$). The cell-treated animals spent significantly longer time in the correct quadrant than the saline-treated animals (Fig. 5B; 33–35 days, $p < 0.05$).

Correlative analysis

There were no correlations among lesion volume, hypoperfusion area, and ventricle size. A mild-to-moderate association between hypoperfusion area and mNSS was detected ($R = 0.24 \sim 0.63$, $p < 0.05$), with a larger hypoperfusion area relating to higher mNSS or worse performance.

Discussion

Treatment of TBI with transplantation of hMSCs was noninvasively and longitudinally investigated using MRI. To reveal the dynamic effects of grafted hMSCs on the injured brain, the progressive evolution of focal lesion, as well as hemodynamic and morphological alteration following TBI, was tracked *in vivo* up to 6 weeks post-TBI. We demonstrated that intravenously transplanted hMSCs benefited the trauma-injured brain by restoring CBF and reducing cerebral tissue loss, which paralleled the improvement of neurological functional performance over the same period.

In the present study, we confirmed that 3D MRI can sensitively and dynamically detect the migration and distribution of SPIO-labeled cells in the host-injured brain. Combining 3D image with T2WI, the labeled cell cluster was distinguished from intracerebral hemorrhage mainly by its distinct MR signal evolution patterns. While the labeled cells produced persistent signal intensity on both 3D image and T2WI within the observation period, the hemorrhagic area showed hypointensity, hypointensity within hyperintensity, and hyperintensity surrounded by peripheral hypointensity on T2WI, depending on the biochemical state of hemoglobin along the time course of hemorrhage (Morris, 2002).

To quantify the perfusion abnormality, a viability threshold for CBF (30mL/100 g/min) derived from experimental stroke was used (Shen et al., 2004). The location and extent of tissue regions with CBF lower than this threshold then represented a hypoperfusion status of the brain. It should be pointed out that the selected threshold, which is much lower than the normal level of CBF in the rat brain ($\sim$140 mL/100g/min) (Shen et al., 2004), can be used to identify the regions with disturbed hemodynamics, but may not necessarily relate to consequent ischemic injury in the traumatized brain due to

distinct differences in pathologies between stroke and trauma (Cunningham et al., 2005). Our longitudinal observation confirmed the previous experimental and clinical reports that TBI-induced hypoperfusion occurred at the lesion site and also in distant non-lesion regions (Bonne et al., 2003; Hofman et al., 2001; Pasco et al., 2007). Compared to a cystic lesion with a remarkable and permanent CBF disturbance, the transient reduction in CBF in these regions after TBI could ultimately diminish at a later chronic stage, such as found 1 year post-injury for rat (Kochanek et al., 2002), due to vascular remodeling of the brain. However, hypoperfusion leads to ischemia, hypoxia, and metabolic disturbances in the brain, all of which increase the susceptibility to neuronal injury (Hossmann, 1993). The extent and duration of this situation affect the tissue fate (Cunningham et al., 2005). The sooner the normal blood supply is restored, the more likely the reduction of ischemic injury. Rapid recovery of blood supply is particularly important for the vulnerable perilesional tissue that is at the highest risk of secondary ischemic neuronal injury (Immonen et al., 2009b, 2010). Our measurements showed that treatment with hMSCs after TBI significantly reduced the hypoperfusion area both in the remote regions and in the tissue regions adjacent to the lesion (Fig. 3). In accordance with the view that perfusion compromise is linked to functional deficits (Bonne et al., 2003; Immonem et al., 2010), we found that the reduction of hypoperfusion area was associated with the augmentation of functional recovery as evaluated by mNSS (compare Fig. 3G with Fig. 5A). Nevertheless, the correlation between hypoperfusion area and mNSS was not strong. A plausible reason for this result may be attributed to the mNSS itself, which is a composite of many neurological tests that are likely not directly related to a single physiological parameter, such as CBF. The dynamic measurements also showed that a significantly reduced hypoperfusion area was detected in the cell-treated group at 3 weeks as compared with 2 days post-TBI and persisted thereafter, while no signs were observed that indicated the amelioration of hypoperfusion in the saline-treated group up to 6 weeks post-injury (Fig. 3G), although the eventual diminution of perfusion disturbance in the remote regions is expected (Kochanek et al., 2002). These results indicated that the grafted hMSCs expedited restoration of CBF. Our data suggested a restorative effect of delayed cell transplantation on vascular remodeling in the trauma-injured brain, supporting a previous finding (Xiong et al., 2009). MSCs have been demonstrated to increase angiogenesis (Xiong et al., 2009) and the level of neurotrophic growth factors (Mahmood et al., 2004a) in the traumatized brain and to facilitate the reconstitution of the blood-brain barrier after a focal injury (Borlongan et al., 2004). Hence, angiogenesis evoked by hMSC engraftment and elevated trophic factors that rescue the impaired vasculature (Borlongan et al., 2004) may play a crucial role in the attenuation of TBI-induced hypoperfusion in both the extent and duration observed in the cell-treated animals.

Ventricular expansion, a structural equel of TBI, reflects global atrophy of the brain (Bigler et al., 1987; Ng et al., 2008). To track *in vivo* the evolution of this morphological abnormality after TBI and compare the temporal profiles between two groups, the lateral ventricles visualized by T2 map were measured in the same structural location at each scan time point for all animals (Fig. 2). Both 3D images and T2 maps were used to accurately delineate the expanded ventricles without contamination of cortical lesion (Fig. 1). As expected, our CCI model produced severe TBI with high incidence of intracranial hemorrhage and pronounced cerebral atrophy as evidenced by notable dilated ventricles (Fig. 2). Our quantitative results showed that treatment with hMSCs led to significantly less enlargement of ventricle size in both the ipsilateral and contralateral sides of the injured brain (Fig. 2I,J). The cell transplantation not only significantly reduced the magnitude, but also the longitudinal rate of ventricular dilation after TBI (Fig. 2I,J). Thus, cerebral tissue was preserved at a relatively early stage as a result of cell therapy. We also noted that the reduced structural abnormality, as evidenced by diminished ventricular expansion, was accompanied by improved functional status (compare Fig. 2I,J with Fig. 5A). Volumetric studies demonstrate that regional and global cerebral atrophy is related to unfavorable functional outcomes (Bigler et al., 1997; Blatter et al., 1997; Sidaros et al., 2009), whereas more tissue preservation is associated with better recovery (Wilde et al., 2005). Mechanisms that may account for cerebral tissue shrinkage after TBI include progressive neuronal loss (Immonen et al., 2009a; Smith et al., 1997) and diffuse axonal injury (Bigler, 1987; Ding et al., 2008; Mamere et al., 2009; Sidaros et al., 2009). As found in the present study, MSCs diminish hemodynamic abnormalities (Fig. 3G) by early restoration of blood flow perfusion to deliver oxygen and glucose, which may rescue neurons at risk from energy deprivation (Immonem et al., 2010). The ability of MSCs to facilitate vascular remodeling (Borlongan et al., 2004), to enhance neurogenesis (Mahmood et al., 2004b), to protect neurons (Wilkins et al., 2009) and to support axonal regeneration (Ankeny et al., 2004), which in turn moderate neuropathological change and white matter degeneration, may contribute to tissue preservation (Fig. 2I,J) and consequent recovery of functional outcome (Fig. 5A) after TBI.

Correlative analysis showed that the extent of TBI-induced hypoperfusion and ventricular expansion appeared independent of the focal lesion volume, indicating the nature of generalized effect of secondary events after TBI. While cell transplantation did not affect the lesion volume (Fig. 1E), the intervention significantly reduced hypoperfusion area (Fig. 3G) and retarded ventricular dilation (Fig. 2I,J). It was of interest to note that these beneficial effects were detected not only in the hemisphere ipsilateral to the impact lesion, but also concurrently in the hemisphere contralateral to the injury site where the grafted cells were seldom found in the host brain (Lu et al., 2001; Mahmood et al., 2001, 2003).

Consistent with the histological findings (Lu et al., 2001; Mahmood et al., 2001, 2003), our dynamic observations demonstrate that systemically administrated hMSCs migrate into the brain within 1 week after engraftment and preferentially accumulate and surround the injured tissue area (Fig. 4). Although only a small percentage of the injected cells entered the parenchyma of the brain (Lu et al., 2001; Mahmood et al., 2001, 2004a), with the majority of them locating in the restricted regions regulated by the injury (Li et al., 2010), the action of these small amounts of cells led to a relatively widespread modification of hemodynamic and structural abnormalities in the traumatized brain (Figs. 2 and 3). The current findings support the concept that the numbers of transplanted hMSCs appear highly insufficient to replace damaged tissues, but provide an *in vivo* source of cytokines and trophic factors under the influence of the injured tissue

that activate endogenous restorative and regenerative processes (Chopp and Li, 2006; Opydo-Chanek, 2007; Parr et al., 2007), resulting in enhanced post-injury brain remodeling. Our *in vivo* measurements illustrate that these cell-induced repairing and healing processes could influence the brain regions distant from the location where the grafted cells predominantly gathered. Cell transplantation, therefore, has the potential to offer an effective therapy targeted for attenuation of secondary injury after TBI that diffusely affects brain.

In summary, treatment with hMSCs following TBI diminishes hemodynamic abnormalities by early restoration and preservation of CBF in the brain regions adjacent to and remote from the impact site, and reduces generalized cerebral atrophy, all of which may contribute to the observed improvement of functional outcome.

Acknowledgments

This work was supported by the National Institute of Neurological Disorders and Stroke (grants P50 NS23393, PO1 NS42345, RO1 NS48349, RO1 NS38292, RO1 NS43324, HL64766) and the Mort and Brigitte Harris Foundation.

Author Disclosure Statement

No conflicting financial interests exist.

References

Ankeny, D.P., McTigue, D.M., and Jakeman, L.B. (2004). Bone marrow transplants provide tissue protection and directional guidance for axons after contusive spinal cord injury in rats. Exp. Neurol. 190, 17–31.

Assaf, Y., Beit-Yannai, E., Shohami, E., Berman, E., and Cohen, Y. (1997). Diffusion- and T2-weighted MRI of closed-head injury in rats: a time course study and correlation with histology. Magn. Reson. Imaging 15, 77–85.

Bigler, E.D. (1987). The clinical significance of cerebral atrophy in traumatic brain injury. Arch. Clin. Neuropsychol. 2, 293–304.

Bigler, E.D., Blatter, D.D., Anderson, C.V., Johnson, S.C., Gale, S.D., Hopkins, R.O., and Burnett, B.M. (1997). Hippocampal volume in normal aging and traumatic brain injury. Am. J. Neuroradiol. 18, 11–23.

Blatter, D.D., Bigler, E.D., Gale, S.D., Johnson, S.C., Anderson, C.V., Burnett, B.M., Ryser, D., Macnamara, S.E., and Bailey, B.J. (1997). MR-based brain and cerebrospinal fluid measurement after traumatic brain injury: correlation with neuropsychological outcome. Am. J. Neuroradiol. 18, 1–10.

Bonne, O., Gilboa, A., Louzoun, Y., Kempf-Sherf, O., Katz, M., Fishman, Y., Ben-Nahum, Z., Krausz, Y., Bocher, M., Lester, H., Chisin, R., and Lerer, B. (2003). Cerebral blood flow in chronic symptomatic mild traumatic brain injury. Psychiatry Res. 124, 141–152.

Borlongan, C.V., Lind, J.G., Dillon-Carter, O., Yu, G., Hadman, M., Cheng, C., Carroll, J., and Hess, D.C. (2004). Intracerebral xenografts of mouse bone marrow cells in adult rats facilitate restoration of cerebral blood flow and blood-brain barrier. Brain Res. 1009, 26–33.

Chopp, M., and Li, Y. (2006). Transplantation of bone marrow stromal cells for treatment of central nervous system diseases. Adv. Exp. Med. Biol. 585, 49–64.

Cunningham, A.S., Salvador, R., Coles, J.P., Chatfield, D.A., Bradley, P.G., Johnston, A.J., Steiner, L.A., Fryer, T.D., Aigbirhio, F.I., Smielewski, P., Williams, G.B., Carpenter, T.A., Gillard, J.H., Pickard, J.D., and Menon, D.K. (2005). Physiological thresholds for irreversible tissue damage in contusional regions following traumatic brain injury. Brain 128, 1931–1942.

Ding, K., Marquez de la Plata, C., Wang, J.Y., Mumphrey, M., Moore, C., Harper, C., Madden, C.J., McColl, R., Whittemore, A., Devous, M.D., and Diaz-Arrastia, R. (2008). Cerebral atrophy after traumatic white matter injury: correlation with acute neuroimaging and outcome. J. Neurotrauma 25, 1433–1440.

Hofman, P.A., Stapert, S.Z., van Kroonenburgh, M.J., Jolles, J., de Kruijk, J., and Wilmink, J.T. (2001). MR imaging, single-photon emission CT, and neurocognitive performance after mild traumatic brain injury. Am. J. Neuroradiol. 22, 441–449.

Hossmann, K.A. (1993). Ischemia-mediated neuronal injury. Resuscitation 26, 225–235.

Immonem, R., Heikkinen, T., Tahtivaara, L., Nurmi, A., Stenius, T.K., Puolivali, J., Tuinstra, T., Phinney, A.L., Van Vliet, B., Yrjanheikki, J., and Grohn, O. (2010). Cerebral blood volume alterations in the perilesional areas in the rat brain after traumatic brain injury—comparison with behavioral outcome. J. Cereb. Blood Flow Metab. 30, 1318–1328.

Immonen, R.J., Kharatishvili, I., Grohn, H., Pitkanen, A., and Grohn, O.H. (2009a). Quantitative MRI predicts long-term structural and functional outcome after experimental traumatic brain injury. Neuroimage 45, 1–9.

Immonen, R.J., Kharatishvili, I., Niskanen, J.P., Grohn, H., Pitkanen, A., and Grohn, O.H. (2009b). Distinct MRI pattern in lesional and perilesional area after traumatic brain injury in rat—11 months follow-up. Exp. Neurol. 216, 29–40.

Kochanek, P.M., Hendrich, K.S., Dixon, C.E., Schiding, J.K., Williams, D.S., and Ho, C. (2002). Cerebral blood flow at one year after controlled cortical impact in rats: assessment by magnetic resonance imaging. J. Neurotrauma 19, 1029–1037.

Li, L., Jiang, Q., Ding, G., Zhang, L., Zhang, Z.G., Ewing, J.R., Knight, R.A., Kapke, A., Soltanian-Zadeh, H., and Chopp, M. (2005). Map-ISODATA demarcates regional response to combination rt-PA and7E3 F(ab')2 treatment of embolic stroke in the rat. J. Magn. Reson. Imaging 21, 726–734.

Li, L., Jiang, Q., Ding, G., Zhang, L., Zhang, Z.G., Li, Q., Panda, S., Lu, M., Ewing, J.R., and Chopp, M. (2010). Effects of administration route on migration and distribution of neural progenitor cells transplanted into rats with focal cerebral ischemia, an MRI study. J. Cereb. Blood Flow Metab. 30, 653–662.

Lu, D., Mahmood, A., Qu, C., Hong, X., Kaplan, D., and Chopp, M. (2007). Collagen scaffolds populated with human marrow stromal cells reduce lesion volume and improve functional outcome after traumatic brain injury. Neurosurgery 61, 596–602.

Lu, D., Mahmood, A., Wang, L., Li, Y., Lu, M., and Chopp, M. (2001). Adult bone marrow stromal cells administered intravenously to rats after traumatic brain injury migrate into brain and improve neurological outcome. Neuroreport 12, 559–563.

MacKenzie, J.D., Siddiqi, F., Babb, J.S., Bagley, L.J., Mannon, L.J., Sinson, G.P., and Grossman, R.I. (2002). Brain atrophy in mild or moderate traumatic brain injury: a longitudinal quantitative analysis. Am. J. Neuroradiol. 23, 1509–1515.

Mahmood, A., Lu, D., and Chopp, M. (2004a). Intravenous administration of marrow stromal cells (MSCs) increases the expression of growth factors in rat brain after traumatic brain injury. J. Neurotrauma 21, 33–39.

Mahmood, A., Lu, D., and Chopp, M. (2004b). Marrow stromal cell transplantation after traumatic brain injury promotes cellular proliferation within the brain. Neurosurgery 55, 1185–1193.

Mahmood, A., Lu, D., Lu, M., and Chopp, M. (2003). Treatment of traumatic brain injury in adult rats with intravenous

administration of human bone marrow stromal cells. Neurosurgery 53, 679–702.

Mahmood, A., Lu, D., Qu, C., Goussev, A., Zhang, Z.G., Lu, C., and Chopp, M. (2007). Treatment of traumatic brain injury in rats with erythropoietin and carbamylated erythropoietin. J. Neurosurg. 107, 392–397.

Mahmood, A., Lu, D., Wang, L., Li, Y., Lu, M., and Chopp, M. (2001). Treatment of traumatic brain injury in female rats with intravenous administration of bone marrow stromal cells. Neurosurgery 49, 1196–1203.

Mamere, A.E., Saraiva, L.A., Matos, A.L., Carneiro, A.A., and Santos, A.C. (2009). Evaluation of delayed neuronal and axonal damage secondary to moderate and severe traumatic brain injury using quantitative MR imaging techniques. Am. J. Neuroradiol. 30, 947–952.

Morris, P.P. (2002). Intracranial hemorrhage, in: *Magnetic Resonance Imaging of the Brain and Spine*, 3rd ed. S.W. Atlas (ed). Lippincott Williams & Wilkins: Philadelphia, pps. 773–832.

Ng, K., Mikulis, D.J., Glazer, J., Kabani, N., Till, C., Greenberg, G., Thompson, A., Lazinski, D., Agid, R., Colella, B., and Green, R.E. (2008). Magnetic resonance imaging evidence of progression of subacute brain atrophy in moderate to severe traumatic brain injury. Arch. Phys. Med. Rehabil. 89, S35–44.

Opydo-Chanek, M. (2007). Bone marrow stromal cells in traumatic brain injury (TBI) therapy: true perspective or false hope? Acta Neurobiol. Exp. 67, 187–195.

Parr, A.M., Tator, C.H., and Keating, A. (2007). Bone marrow-derived mesenchymal stromal cells for the repair of central nervous system injury. Bone Marrow Transplant. 40, 609–619.

Pasco, A., Lemaire, L., Franconi, F., Lefur, Y., Noury, F., Saint-Andre, J.P., Benoit, J.P., Cozzone, P.J., and Le Jeune, J.J. (2007). Perfusional deficit and the dynamics of cerebral edemas in experimental traumatic brain injury using perfusion and diffusion-weighted magnetic resonance imaging. J. Neurotrauma 24, 1321–1330.

Shen, Q., Ren, H., Fisher, M., Bouley, J., and Duong, T.Q. (2004). Dynamic tracking of acute ischemic tissue fates using improved unsupervised ISODATA analysis of high-resolution quantitative perfusion and diffusion data. J. Cereb. Blood Flow Metab. 24, 887–897.

Sidaros, A., Skimminge, A., Liptrot, M.G., Sidaros, K., Engberg, A.W., Herning, M., Paulson, O.B., Jernigan, T.L., and Rostrup, E. (2009). Long-term global and regional brain volume changes following severe traumatic brain injury: a longitudinal study with clinical correlates. Neuroimage 44, 1–8.

Smith, D.H., Chen, X.H., Pierce, J.E., Wolf, J.A., Trojanowski, J.Q., Graham, D.I., and McIntosh, T.K. (1997). Progressive atrophy and neuron death for one year following brain trauma in the rat. J. Neurotrauma 14, 715–727.

Soares, H.D., Thomas, M., Cloherty, K., and McIntosh, T.K. (1992). Development of prolonged focal cerebral edema and regional cation changes following experimental brain injury in the rat. J. Neurochem. 58, 1845–1852.

Stoica, B.A., and Faden, A.I. (2010). Cell death mechanisms and modulation in traumatic brain injury. Neurotherapeutics 7, 3–12.

Trivedi, M.A., Ward, M.A., Hess, T.M., Gale, S.D., Dempsey, R.J., Rowley, H.A., and Johnson, S.C. (2007). Longitudinal changes in global brain volume between 79 and 409 days after traumatic brain injury: relationship with duration of coma. J. Neurotrauma 24, 766–771.

Wilde, E.A., Hunter, J.V., Newsome, M.R., Scheibel, R.S., Bigler, E.D., Johnson, J.L., Fearing, M.A., Cleavinger, H.B., Li, X., Swank, P.R., Pedroza, C., Roberson, G.S., Bachevalier, J., and Levin, H.S. (2005). Frontal and temporal morphometric findings on MRI in children after moderate to severe traumatic brain injury. J. Neurotrauma 22, 333–344.

Wilkins, A., Kemp, K., Ginty, M., Hares, K., Mallam, E., and Scolding, N. (2009). Human bone marrow-derived mesenchymal stem cells secrete brain-derived neurotrophic factor which promotes neuronal survival in vitro. Stem Cell Res. (in press).

Xiong, Y., Qu, C., Mahmood, A., Liu, Z., Ning, R., Li, Y., Kaplan, D.L., Schallert, T., and Chopp, M. (2009). Delayed transplantation of human marrow stromal cell-seeded scaffolds increases transcallosal neural fiber length, angiogenesis, and hippocampal neuronal survival and improves functional outcome after traumatic brain injury in rats. Brain Res. 1263, 183–191.

Xu, Y., McArthur, D.L., Alger, J.R., Etchepare, M., Hovda, D.A., Glenn, T.C., Huang, S., Dinov, I., and Vespa, P.M. (2010). Early nonischemic oxidative metabolic dysfunction leads to chronic brain atrophy in traumatic brain injury. J. Cereb. Blood Flow Metab. 30, 883–894.

Ziebell, J.M., and Morganti-Kossmann, M.C. (2010). Involvement of pro- and anti-inflammatory cytokines and chemokines in the pathophysiology of traumatic brain injury. Neurotherapeutics 7, 22–30.

Address correspondence to:
Quan Jiang, Ph.D.
Education & Research Building, B126
Neurology Department
Henry Ford Hospital
2799 West Grand Boulevard
Detroit, MI 48202

E-mail: QJIANG1@hfhs.org